Josephson parametric phase-locked oscillator and its application to dispersive readout of superconducting qubits

Z. R. Lin,[1] K. Inomata,[1] K. Koshino,[2] W. D. Oliver,[3] Y. Nakamura,[4,1] J. S. Tsai,[1,5] and T. Yamamoto[1,5,*]

[1]*RIKEN Center for Emergent Matter Science (CEMS), Wako, Saitama 351-0198, Japan*
[2]*College of Liberal Arts and Sciences, Tokyo Medical and Dental University, Ichikawa, Chiba 272-0827, Japan*
[3]*MIT Lincoln Laboratory, Lexington, Massachusetts 02420, USA*
[4]*Research Center for Advanced Science and Technology (RCAST),*
The University of Tokyo, Meguro-ku, Tokyo 153-8904, Japan
[5]*NEC Smart Energy Research Laboratories, Tsukuba, Ibaraki 305-8501, Japan*
(Dated: July 29, 2014)

The parametric phase-locked oscillator (PPLO),[1] also known as a parametron,[2] is a resonant circuit in which one of the reactances is periodically modulated. It can detect, amplify, and store binary digital signals in the form of two distinct phases of self-oscillation. Indeed, digital computers using PPLOs based on a magnetic ferrite ring or a varactor diode as its fundamental logic element were successfully operated in 1950s and 1960s.[2] More recently, basic bit operations have been demonstrated in an electromechanical resonator,[3] and an Ising machine based on optical PPLOs has been proposed.[4] Here, using a PPLO realized with Josephson-junction circuitry, we demonstrate the demodulation of a microwave signal digitally modulated by binary phase-shift keying. Moreover, we apply this demodulation capability to the dispersive readout of a superconducting qubit. This readout scheme enables a fast and latching-type readout, yet requires only a small number of readout photons in the resonator to which the qubit is coupled, thus featuring the combined advantages of several disparate schemes.[5,6] We have achieved high-fidelity, single-shot, and non-destructive qubit readout with Rabi-oscillation contrast exceeding 90%, limited primarily by the qubit's energy relaxation.

Our PPLO is implemented by a superconducting coplanar waveguide (CPW) resonator defined by a coupling capacitor C_{in}^{PO} and a dc-SQUID termination (Fig. 1a; see Supplementary Information for the details of the device). The dc-SQUID, working as a controllable inductor, makes the resonant frequency of the resonator ω_0^{PO} dependent on an external magnetic flux through the SQUID loop Φ_{sq} (Ref. 7). Thus, the application of a microwave field at a frequency ω_p and a power P_p to the pump line, which is inductively coupled to the SQUID loop, modulates the resonant frequency around its static value. This device has previously been operated as a Jopsehson parametric amplifier[8,9] (JPA): The signal at

$\sim \omega_0^{PO}$ entering the resonator obtains a parametric gain produced by the pump at $\omega_p \sim 2\omega_0^{PO}$ and is reflected back along the signal line. This device also works as a parametric oscillator when it is operated at P_p above the threshold P_{p0} determined by the photon decay rate of the resonator.[10,11] Namely, it generates an output microwave field at $\omega_p/2$ even without any signal injection. The output can be one of the two degenerate oscillatory states (0π and 1π states) which differ solely by a relative phase shift π.

When an additional signal at $\sim \omega_p/2$ with a power P_s^{PO}, which we call the locking signal (LS), is injected into the parametric oscillator, the degeneracy of the two oscillatory states is lifted.[12] Such degeneracy lifting has been demonstrated in other physical systems such as magneto-optically trapped cold atoms[13] and electromechanical systems.[14] To understand the dynamics, we consider the Hamiltonian of the PPLO including a signal port for the LS and a fictitious loss port for internal loss of the resonator, namely,

$$\mathcal{H}/\hbar = \omega_0^{PO} a^\dagger a + \frac{\kappa}{2}\sqrt{\frac{P_p}{P_{p0}}}\cos(2\omega_0^{PO}t)(a+a^\dagger)^2$$

$$+\gamma(a+a^\dagger)^4 + \int dk\left[v_b k b_k^\dagger b_k + i\sqrt{\frac{v_b\kappa_1}{2\pi}}\left(a^\dagger b_k - b_k^\dagger a\right)\right]$$

$$+ \int dk\left[v_c k c_k^\dagger c_k + i\sqrt{\frac{v_c\kappa_2}{2\pi}}\left(a^\dagger c_k - c_k^\dagger a\right)\right], \qquad (1)$$

where γ represents the nonlinearity of the Josephson junction (JJ), a is the annihilation operator for the resonator, b_k (c_k) is the annihilation operator for the photon in the signal (loss) port with a wave number k and a velocity v_b (v_c), κ_1 (κ_2) represents the coupling strength between the resonator and the signal (loss) port, and $\kappa = \kappa_1 + \kappa_2$. The equations of motion for the classical resonator field in a frame rotating at ω_0^{PO} are obtained from the Hamiltonian by setting $\langle a \rangle = [q_x(t) - iq_y(t)]e^{-i\omega_0^{PO}t}$ and are given by (Ref. 15; also see Supplementary Information for derivation)

$$\frac{dq_x}{dt} = -\frac{\kappa}{2}q_x + \frac{\partial g}{\partial q_y}, \qquad (2)$$

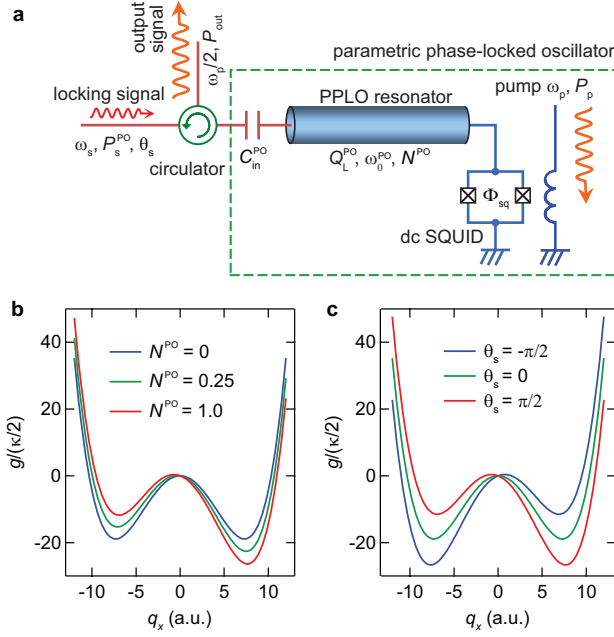$$\frac{dq_y}{dt} = -\frac{\kappa}{2}q_y - \frac{\partial g}{\partial q_x}, \qquad (3)$$

FIG. 1: **Parametric phase-locked oscillator. a,** Schematic of the device. The application of a pump microwave field at $\omega_p \sim 2\omega_0^{PO}$ with a power P_p above the threshold generates an output signal at $\omega_p/2$ with a power P_{out}. Here, ω_0^{PO} is the static resonant frequency of the PPLO resonator, and ω_s, P_s^{PO} and θ_s represent the frequency, power and phase of the locking signal, respectively. C_{in}^{PO} represents the coupling capacitance between the resonator and the feedline, and Φ_{sq} represents the magnetic flux penetrating the SQUID loop. **b,** Cross-section of the Hamiltonian $g(q_x, 0)$ in the rotating frame for various powers and a fixed phase ($\theta_s = \pi/2$) of the locking signal. Here, the LS power is represented by the mean photon number in the PPLO resonator, $N^{PO} = 4P_s^{PO}Q_L^{PO^2}/(\hbar\omega_0^{PO^2}Q_e^{PO})$. The pump power P_p/P_{p0} is fixed at 2.0. Two minima correspond to 0π and 1π states of the phase-locked oscillations. **c,** Same as **b**, but for $N^{PO} = 1$ and various values of θ_s.

where

$$g(q_x, q_y) = \frac{\kappa}{4}\sqrt{\frac{P_p}{P_{p0}}}(q_y^2 - q_x^2) - 3\gamma(q_x^2 + q_y^2)^2$$
$$+ \sqrt{\kappa_1}|E_s|(q_y\cos\theta_s - q_x\sin\theta_s), \quad (4)$$

and $|E_s| = \sqrt{P_s^{PO}/\hbar\omega_0^{PO}}$ and θ_s are the amplitude and phase of the LS, respectively. In the absence of the first term (oscillator's friction term) on the right-hand side, Eqs. 2 and 3 are in the form of Hamilton's equations of motion with the Hamiltonian $g(q_x, q_y)$, whose minima correspond to 0π and 1π states.[15] As shown in Fig. 1b, $g(q_x, 0)$ is symmetric with respect to q_x when there is no LS ($|E_s| = 0$), and 0π and 1π states are degenerate. When we apply LS, it gives a tilt to the double well, which is proportional to $|E_s|\sin\theta_s$ (Figs. 1b and 1c). This lifts the degeneracy, and the PPLO, initially at $q_x, q_y \sim 0$, preferably evolves into one of the two states. This is how

the amplitude and the phase of LS control the output state of the PPLO.

Now we show the experimental results. Figure 2a shows the output power of the PPLO operated at $\omega_p = 2\omega_0^{PO} = 2\pi \times 21.014$ GHz (solid blue circles) as a function of P_p in the absence of LS injection. For each P_p, the microwave field is continuously applied to the pump port, and the output signal at $\omega_p/2$ is measured by a spectrum analyzer. Note that power levels stated in this work are referred to the corresponding ports on the chip. The steep increase of the output power at $P_p \sim -65$ dBm indicates the onset of the parametric oscillation. This is further confirmed by detecting the response to the pulsed pump. Figure 2b shows the histogram of the demodulated amplitude and phase of the output signal plotted in the quadrature (IQ) plane. For each application of the pump pulse with an amplitude of $P_p = -62$ dBm, we recorded the output pulse and extracted its amplitude and phase by averaging for 100 ns. The two distribution peaks correspond to 0π and 1π states. They have equal amplitude, but different phases shifted by π, and are observed with equal probabilities as expected.

Next we perform a similar measurement, but include LS injection. Figure 2c shows the histogram of the demodulated phase of the output signal as a function of the LS phase. While continuously injecting LS with a phase θ_s and a power $P_s^{PO} = -125$ dBm, we applied a pulsed pump with the same duration and the amplitude as in Fig. 2b, and extracted the phase of the output signal. As exemplified by the cross-section along the dashed line, the probabilities of obtaining the two states are no longer equal and depend on θ_s. In Fig. 2d, we plot the probability of 0π state as a function of θ_s for different P_s^{PO}'s. The probability shows sinusoidal dependence when P_s^{PO} is small. As we increase P_s^{PO}, the modulation amplitude ($\Delta P_{0\pi}$) also increases, and finally reaches unity. We define $(1 - \Delta P_{0\pi})/2$ as a non-locking error, and plot it as a function of P_s^{PO} in Fig. 2e by blue circles. When P_s^{PO} is larger than ~ -125 dBm, the non-locking error becomes negligible. We also simulated the non-locking error by solving a master equation[16] based on the Hamiltonian (Eq. 1), and plot it by red curve. (For details, see Supplementary Information.) The only assumption here is the pump threshold P_{p0}, which is set to be -64.0 dBm. The agreement between the theory and the experiment is fairly good.

The above result indicates the PPLO is a phase detector sensitive to very small microwave powers of the order of a femtowatt. To demonstrate this, we generate a signal digitally modulated by binary phase-shift keying (BPSK), a scheme commonly used in modern telecommunications,[17] and demodulate it using a PPLO. Figure 3a shows the sequence of the experiment. The generated signal has a fixed carrier frequency of 10.503 GHz, fixed power of -125 dBm, and a phase which is digitally modulated by π every 500 ns. This means that the signal carries alternating binary bits with a baseband frequency of 2 MHz. Synchronously, we apply pump pulses with the
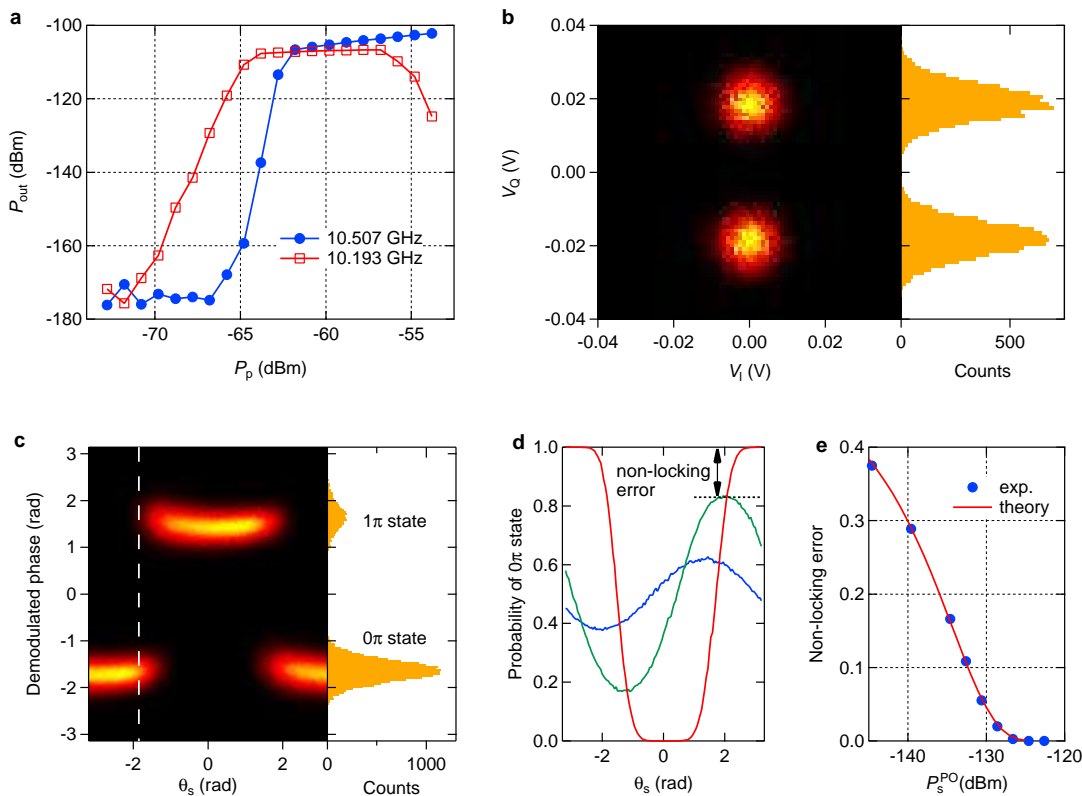
FIG. 2: **Output of the parametric phase-locked oscillator (PPLO). a,** Output signal power as a function of P_p at $\omega_0^{PO}/2\pi = 10.507$ GHz (solid blue circles) and $\omega_0^{PO}/2\pi = 10.193$ GHz (open red squares). The steep increase of the output power indicates onset of the parametric oscillation. For **b-e**, $\omega_0^{PO}/2\pi$ is set to be 10.507 GHz. **b,** Histogram of the amplitude and phase of the output signal plotted in the quadrature (IQ) plane (left panel), and its projection onto the V_Q axis (right panel). The pulsed pump with a duration of 1.6 μs and an amplitude of -62 dBm is applied 1.6×10^4 times in total. No locking signal (LS) is applied. **c,** Histogram of the output-signal phase as a function of the LS phase θ_s (left panel) and its cross-section along the dashed line (right panel). The same pulsed pump as in **b** is applied 2.0×10^4 times for each θ_s. LS is continuously applied with the power of -125 dBm. **d,** Probability of 0π state as a function of θ_s for P_s of -145 dBm (blue), -135 dBm (green), and -125 dBm (red). **e,** Non-locking error as a function of the LS power P_s^{PO}. Solid blue circles represent the experimental data, and the red curve is the result of a simulation based on the master equation.

duration of 300 ns and the amplitude of -62 dBm. Figure 3b shows the superposed time traces of the PPLO output. It shows successful demodulation of the input signal except rare errors as exemplified in the figure. We sent a total of 2.4×10^4 bits and detected 4 errors, corresponding to the error rate of 1.7×10^{-4}.

Now we apply this phase discrimination capability to the dispersive readout of a qubit. Figure 4a shows the measurement setup. A chip containing a 3-JJ superconducting flux qubit capacitively coupled to a CPW resonator (readout resonator) is connected to the PPLO via circulators. The flux qubit is biased at $\Phi_q = 0.5\Phi_0$, where the qubit transition frequency from $|0\rangle$ to $|1\rangle$ states is 5.510 GHz. Figure 4b shows the phase rotation of the reflection coefficient around the resonant frequency of the readout resonator (ω_0^r) when the qubit is in $|0\rangle$ (blue) and $|1\rangle$ (green). The shift between the two curves is due to

the dispersive coupling between the qubit and the readout resonator.[18] We set ω_s to be 10.193 GHz, such that the qubit states are mapped onto two phases of the reflected microwave differing by π.

We discriminate the two states by using the PPLO and the pulse sequence shown in Fig. 4a. We set $\omega_0^{PO} = \omega_s$, $\omega_p = 2\omega_s$ (corresponding to open red squares in Fig. 2a), and $P_p = -65$ dBm. Figure 4c shows the probability of detecting the 0π state as a function of the phase of the readout microwave pulse θ_s (similar to Fig. 2d) with the qubit control π pulse off (blue) and on (green). The power of the readout microwave field at the input of the readout resonator P_s^r is -120 dBm, which corresponds to the mean photon number in the readout resonator $N^r = 4P_s^r Q_L^{r\,2}/(\hbar\omega_0^{r\,2}Q_e^r) = 5.5$. Reflecting the π-phase difference of the reflected microwave field, the two curves are out of phase, and their difference corresponds to the
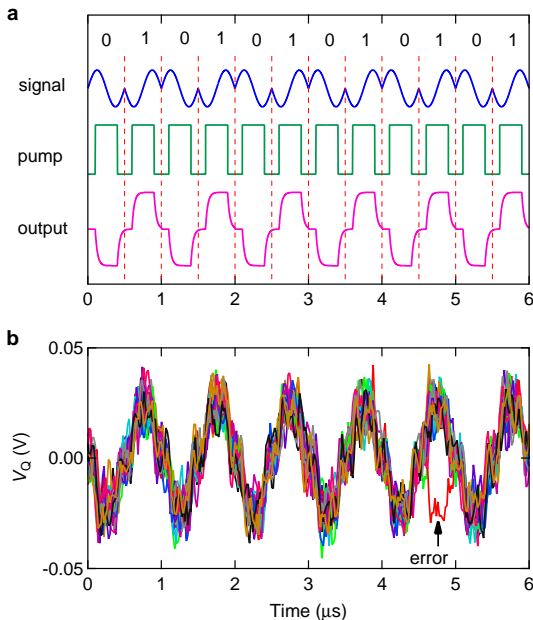
FIG. 3: **Demodulation of BPSK signal. a,** Pulse sequence. BPSK signal at 10.503 GHz with an amplitude of -125 dBm is generated by mixing the 10.553 GHz signal and 50 MHz IF signal (blue curve). Phase of the IF signal is digitally modulated by π (corresponding to bit "0" and bit "1") every 500 ns, and the pulsed pump (green curve) is synchronously applied. The magenta curve represents the expected output of the PPLO. **b,** Examples of the demodulated signal. Twenty individual time traces are superposed.

fidelity of the qubit readout, which is maximized at -2.0 rad and 1.2 rad to be 89%.

We further maximized the fidelity by tuning t_{p} and adding a short spike in the beginning of the readout pulse, and measured Rabi oscillations as shown in Fig. 4d, where the length t_{c} and the amplitude $\sqrt{P_{\mathrm{c}}}$ of the qubit control pulse are swept. Figure 4e shows the Rabi-oscillation measurement along the dashed line in Fig. 4d. The contrast of the Rabi oscillations is 90.7%. We attribute the sources of the error to incomplete initialization of the qubit by 2.6% and to qubit energy relaxation (including the gate error of the π pulse), which adds 6.7%. Note that the non-zero minimum of the blue curve in Fig. 4c is due to incomplete initialization of the qubit and not the non-locking error. The non-locking error is confirmed to be negligible for both states of the qubit (see details for Supplementary Information).

As stated above, N^{r} of 5.5 is large enough to make the non-locking error of PPLO negligible. It is at the same time small enough for the qubit to avoid readout backaction. By sweeping t_{p}, we can measure T_1 of the qubit, while populating photons in the readout resonator. It is measured to be 690 ns (see Supplementary Information), which agrees with T_1 obtained from the indepen-

dent ensemble-averaged measurement using a standard pulse sequence, namely, a π pulse followed by delayed readout. This indicates the nondestructive character of the present readout scheme.

Another characteristic of the present readout scheme is its latching property. Once the qubit state is mapped to the oscillator state of PPLO, the information can be maintained, regardless of a subsequent qubit state transition, as long as the pump is turned on. We demonstrate this in Fig. 4f, in which the readout fidelity is plotted as a function of t_{d}. Even at $t_{\mathrm{d}} = 6$ μs, at which the qubit has totally decayed, we do not lose readout fidelity.

The present scheme enables fast, latching-type and single-shot readout of the qubit. In this sense, it is similar to schemes using a Josephson bifurcation amplifier,[5] Josephson chirped amplifier,[19] and period-doubling bifurcation,[20] where the qubit is directly coupled to a nonlinear resonator. However, in the present scheme, the mean photon number in the resonator to which the qubit is coupled can be kept small (of order unity) regardless of the result of the readout. In this sense, it is similar to schemes where a qubit is coupled to a linear resonator, followed by an ultra low-noise amplifier such as JPA to achieve single-shot readout.[9] Thus, the present scheme has combined advantages of both linear and nonlinear resonators, and can be useful in quantum error-correction protocols such as the surface code.[21]

Author Contributions T.Y. and Z.R.L. conceived the experiment and wrote the manuscript. Z.R.L. performed the measurement and analyzed the data. K.I. fabricated the qubit device and helped the measurement and the analysis. T.Y. designed PPLO, which was fabricated at the group of W.D.O. K.K. and T.Y. developed the theory and performed numerical simulations. All authors contributed to the discussion of the results and helped editing the manuscript.
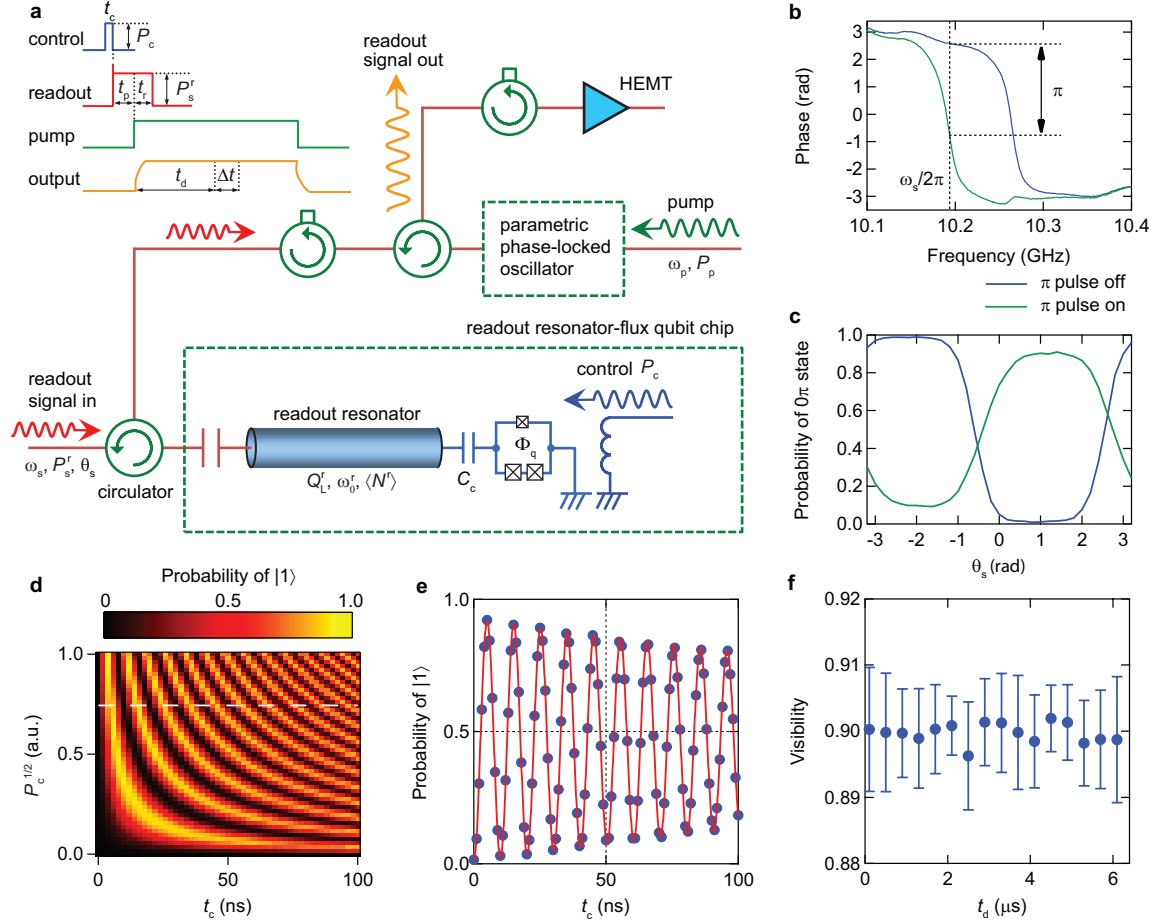
FIG. 4: **Qubit readout using PPLO. a,** Measurement setup and pulse sequence. A 3-JJ superconducting flux qubit biased at $\Phi_q = \Phi_0/2$ is capacitively ($C_c = 4$ fF) coupled to a CPW resonator. Here, ω_0^r and N^r represent the resonant frequency and the mean photon number of the readout resonator, respectively. The internal (Q_i^r) and external (Q_e^r) quality factors are 2.5×10^4 and 630, respectively, resulting in the loaded quality factor Q_L^r of 620. In the pulse sequence, Δt (=100 ns) represents the data-acquisition time to extract the phase, and P_s^r and P_c represent the power of the readout and the qubit-control pulses, respectively. A short spike was added in the readout pulse to improve the readout fidelity. In **c** to **f**, we applied the pulse sequence 1×10^4 times to obtain the probability. **b,** Frequency dependence of the phase of the reflection coefficient of the readout resonator with qubit-control π pulse on (green) and off (blue). **c,** Probability of the PPLO 0π state as a function of the readout-signal phase θ_s with the qubit-control π pulse on (green) and off (blue). Here, $t_c = 10$ ns, $t_p = 50$ ns, $t_r = 50$ ns, and $t_d = 300$ ns. **d,** Rabi oscillations measured with $t_p = 30$ ns, $t_r = 50$ ns, and $t_d = 300$ ns. **e,** Rabi oscillations along the dashed line in **d**. Red curve represents a fit with an exponentially damped sinusoidal function. **f,** Visibility as a function of t_d. Here, $t_c = 10$ ns, $t_p = 30$ ns, and $t_r = 50$ ns. The error bars represents the standard deviation in five identical measurements.

[1] Onyshkevych, L. S., Kosonocky, W. F. & Lo, A. W. Parametric phase-locked oscillator — characteristics and applications to digital systems. *Trans. Inst. Radio Engrs.* **EC-8**, 277-286 (1959).

[2] Goto, E. The parametron, a digital computing element which utilizes parametric oscillation. *Proc. Inst. Radio Engrs.* **47**, 1304-1316 (1959).

[3] Mahboob, I. & Yamaguchi, H. Bit storage and bit flip operations in an elecromechanical oscillator. *Nat. Nanotechnol.* **3**, 275 (2008).

[4] Wang, Z., Marandi, A., Wen, K., Byer, R. L. & Yamamoto, Y. Coherent Ising machine based on degenerate optical parametric oscillators. *Phys. Rev. A* **88**, 063853 (2013).

[5] Siddiqi, I. *et al.* Dispersive measurements of superconducting qubit coherence with a fast latching readout. *Phys. Rev. B* **73**, 054510 (2006).

[6] Vijay, R., Slichter, D. H. & Siddiqi, I. Observation of quantum jumps in a superconducting artificial atom. *Phys. Rev. Lett.* **106**, 110502 (2011).

[7] Wallquist, M., Shumeiko, V. S. & Wendin, G. Selective coupling of superconducting charge qubits mediated by a tunable stripline cavity. *Phys. Rev. B* **74**, 224506 (2006).

[8] Yamamoto, T. *et al.* Flux-driven Josephson parametric amplifier. *Appl. Phys. Lett.* **93**, 042510 (2008).

[9] Lin, Z. R. *et al.* Single-shot readout of a superconducting flux qubit with a flux-driven Josephson parametric amplifier. *Appl. Phys. Lett.* **103**, 132602 (2013).

[10] Wilson, C. M. *et al.* Photon generation in an electromagnetic cavity with a time-dependent boundary. *Phys. Rev. Lett.* **105**, 233907 (2010).

[11] Krantz, P. *et al.* Investigation of nonlinear effects in Josephson parametric oscillators used in circuit quantum electrodynamics. *New Journal of Physics* **15**, 105002 (2013).

[12] Ryvkine, D. & Dykman, M. I. Resonant symmetry lifting in a parametrically modulated oscillator. *Phys. Rev. E* **74**, 061118 (2006).

[13] Kim, Y. *et al.* Observation of resonant symmetry lifting by an effective bias field in a parametrically modulated atomic trap. *Phys. Rev. A* **82**, 063407 (2010).

[14] Mahboob, I., Froitier, C. & Yamaguchi, H. A symmetry-breaking electromechanical detector. *Appl. Phys. Lett.* **96**, 213103 (2010).

[15] Dykman, M. I., Maloney, C. M., Smelyanskiy, V. N. & Silverstein, M. Fluctuational phase-flip transitions in parametrically driven oscillators. *Phys. Rev. E* **57**, 5202–5212 (1998).

[16] Johansson, J., Nation, P. & Nori, F. Qutip 2: A Python framework for the dynamics of open quantum systems. *Computer Physics Communications* **184**, 1234 – 1240 (2013).

[17] Anderson, J. B., Aulin, T. & Sundberg, C.-E. *Digital Phase Modulation* (Plenum Press, New York, 1986).

[18] Inomata, K., Yamamoto, T., Billangeon, P.-M., Nakamura, Y. & Tsai, J. S. Large dispersive shift of cavity resonance induced by a superconducting flux qubit in the straddling regime. *Phys. Rev. B* **86**, 140508 (2012).

[19] Naaman, O., Aumentado, J., Friedland, L., Wurtele, J. S. & Siddiqi, I. Phase-locking transition in a chirped superconducting Josephson resonator. *Phys. Rev. Lett.* **101**, 117005 (2008).

[20] Zorin, A. B. & Makhlin, Y. Period-doubling bifurcation readout for a Josephson qubit. *Phys. Rev. B* **83**, 224506 (2011).

[21] Fowler, A. G., Mariantoni, M., Martinis, J. M. & Cleland, A. N. Surface codes: Towards practical large-scale quantum computation. *Phys. Rev. A* **86**, 032324 (2012).

Supplementary information: Josephson parametric phase-locked oscillator and its application to dispersive readout of superconducting qubits

Z. R. Lin,[1] K. Inomata,[1] K. Koshino,[2] W. D. Oliver,[3] Y. Nakamura,[4,1] J. S. Tsai,[1,5] and T. Yamamoto[1,5,∗]

[1]RIKEN Center for Emergent Matter Science (CEMS), Wako, Saitama 351-0198, Japan
[2]College of Liberal Arts and Sciences, Tokyo Medical and Dental University, Ichikawa, Chiba 272-0827, Japan
[3]MIT Lincoln Laboratory, Lexington, Massachusetts 02420, USA
[4]Research Center for Advanced Science and Technology (RCAST),
The University of Tokyo, Meguro-ku, Tokyo 153-8904, Japan
[5]NEC Smart Energy Research Laboratories, Tsukuba, Ibaraki 305-8501, Japan

I. EXPERIMENTAL DETAILS

A. Images of the Josephson parametric phase-locked oscillator

Figure S1a shows the device image of the parametric phase-locked oscillator (PPLO). The device consists of a quarter wavelength (cavity length 2.6 mm) coplanar waveguide (CPW) resonator with a dc-SQUID termination and a pump line inductively coupled to the SQUID loop (mutual inductance $M \sim 1.0$ pH). The critical current of the Josephson junction of the SQUID is estimated to be 3.1 μA for each junction from the fitting shown in Fig. S6. The device was fabricated by the planarized niobium trilayer process at MIT Lincoln laboratory. The resonator and the pump line are made of 150-nm-thick niobium film sputtered on a Si substrate covered by 500-nm-thick SiO_2 layer. Figure S1b shows the magnified image of the coupling capacitance between the microwave feedline and the resonator C_{in}^{PO}, which is designed to be 15 fF. The internal and external quality factors are measured to be 5200 and 340, respectively at $\omega_0^{PO}/2\pi = 10.507$ GHz, which give the loaded quality factor Q_L^{PO} of 320. Figures S1c and d show the magnified optical image and the scanning electron micrograph of the dc-SQUID part, respectively.

B. Error budget of the Rabi-oscillation contrast

In the main article, we show Rabi oscillations with a contrast of 90.7%. Here, we present our analysis on the loss of the contrast. Possible sources of the error are (i) incomplete initialization of the qubit, (ii) insufficient power of the locking signal (LS), and (iii) qubit energy relaxation (including the gate error in the qubit-control π pulse).

The error from the first source (incomplete initialization) is estimated from the direct measurement of the background qubit excitation by operating the device as Josephson parametric amplifier (JPA) [1], and found to be 2.6%. Half of this is equal to the non-zero minimum of the blue curve in Fig. 4c in the main article. This indicates that the error from the second source (non-locking error) is negligible at least when the qubit is in state $|0\rangle$.

Non-locking error is also estimated from the measurement result shown in Fig. S2, which is similar to the measurement shown in Fig. 2e in the main article, and found to be negligible for both of the qubit states. Minimum probability of 1π state decreases as we increase P_s^{PO} and saturates at the level determined by the background qubit excitation when P_s^{PO} is larger than ~ -124 dBm.

The microwave powers injected into the PPLO when the qubit is in $|0\rangle$ state and in $|1\rangle$ state are shown in the figure as P_s^0 and P_s^1, respectively. Because of the dispersive shift in ω_0^r and finite internal loss of the readout resonator, P_s^1 is slightly lower than P_s^0 which is set at -122.5 dBm. P_s^1 is estimated by directly measuring the amplitude of the reflected microwave when the qubit is excited to $|1\rangle$ state. Figure S3 shows the histograms of the voltage of the reflected readout pulse when the qubit-control π pulse is not applied (a) and is applied (b) to the qubit. The reflected voltage is measured by a single-shot readout using JPA [1]. The peak in Fig. S3a corresponds to the qubit state $|0\rangle$, while the right peak in Fig. S3b corresponds to the qubit state $|1\rangle$. By fitting the peaks with Gaussian functions, we extract the voltage of the reflected readout pulse when the qubit is in $|0\rangle$ state and in $|1\rangle$ state, which we call V_0 and V_1, respectively. V_i and P_s^i (i=0,1) satisfy the following relation

$$\frac{P_s^0 G(P_s^0)}{P_s^1 G(P_s^1)} = \left(\frac{V_0}{V_1}\right)^2,\tag{S1}$$

∗t-yamamoto@fe.jp.nec.com

where G represents the power gain of the JPA. Note that G is not necessarily independent of the input power when the input power is high, and we measured it independently (data not shown). From Eq. S1, P_s^1 is estimated to be -123.0 dBm.

The rest of the error is attributable to the third source (qubit relaxation). The energy relaxation time T_1 of the qubit is measured to be 690 ns (see below). Assuming $1 - \exp(-t_w/T_1) = 0.067$, $t_w = 48$ ns is obtained, which is close to the sum of t_c, t_p and the response time of PPLO measured to be ~ 10 ns (Fig. S4).

C. Qubit energy relaxation time

Figure S5 shows the probability of 0π state as a function of t_p when the qubit-control π pulse is turned off and on. We fit the data (π pulse on) from $t_p = 40$ ns to 3 μs with an exponential function, and obtain the time constant of 690 ns. This agrees with the qubit energy relaxation time T_1 of 694 ns obtained from an independent ensemble-averaged measurement using standard pulse sequence for T_1 measurement, namely, π pulse followed by the delayed readout. Small decay of the data without π pulse is possibly due to the qubit excitation induced by the readout pulse.

II. THEORY AND SIMULATIONS

A. Hamiltonian and equations of motion

The Hamiltonian of the PPLO including a signal port for the locking signal (LS) and a fictitious loss port for internal loss of the resonator is given by [2]

$$\mathcal{H}(t) = \mathcal{H}_{\mathrm{sys}}(t) + \mathcal{H}_{\mathrm{sig}} + \mathcal{H}_{\mathrm{loss}}, \tag{S2}$$

$$\mathcal{H}_{\mathrm{sys}}(t)/\hbar = \omega_0^{\mathrm{PO}}\left[a^\dagger a + \epsilon \cos(\omega_p t)(a + a^\dagger)^2\right] + \gamma(a + a^\dagger)^4, \tag{S3}$$

$$\mathcal{H}_{\mathrm{sig}}/\hbar = \int dk\left[v_b k b_k^\dagger b_k + \mathrm{i}\sqrt{\frac{v_b \kappa_1}{2\pi}}\left(a^\dagger b_k - b_k^\dagger a\right)\right], \tag{S4}$$

$$\mathcal{H}_{\mathrm{loss}}/\hbar = \int dk\left[v_c k c_k^\dagger c_k + \mathrm{i}\sqrt{\frac{v_c \kappa_2}{2\pi}}\left(a^\dagger c_k - c_k^\dagger a\right)\right], \tag{S5}$$

where ω_0^{PO} is the static resonant frequency of the PPLO, ω_p and ϵ represent the frequency and magnitude of the parametric modulation, respectively, γ represents the nonlinearity of the Josephson junction (JJ), a is the annihilation operator for the resonator, b_k (c_k) is the annihilation operator for the photon in the signal (loss) port with a wave number k and a velocity v_b (v_c), and κ_1 (κ_2) represents the coupling strength between the resonator and the signal (loss) port. The operators satisfy the following commutation rules: $[a, a^\dagger] = 1$, $[b_k, b'_k{}^\dagger] = \delta(k - k')$, and $[c_k, c'_k{}^\dagger] = \delta(k - k')$. The coupling constants κ_1 and κ_2 are related to the external and internal quality factors of the resonator as follows: $\kappa_1 = \omega_0^{\mathrm{PO}}/Q_{\mathrm{e}}^{\mathrm{PO}}$ and $\kappa_2 = \omega_0^{\mathrm{PO}}/Q_{\mathrm{i}}^{\mathrm{PO}}$. Below we consider the case where $\omega_p = 2\omega_0^{\mathrm{PO}}$.

From the Heisenberg equations of motion for b_k, we obtain

$$\frac{db_k(t)}{dt} = -\mathrm{i}v k b_k(t) - \sqrt{\frac{v\kappa_1}{2\pi}}a(t). \tag{S6}$$

By solving this differential equation formally, we have

$$b_k(t) = e^{-\mathrm{i}v k t}b_k(0) - \sqrt{\frac{v\kappa_1}{2\pi}}\int_0^t e^{-\mathrm{i}v k(t-t')}a(t')dt'. \tag{S7}$$

We introduce the real-space representation of the waveguide field by $\widetilde{b}_r = (2\pi)^{-1/2}\int dk e^{\mathrm{i}kr}b_k$. In this representation, the waveguide field interacts with the resonator at $r = 0$ and the $r < 0$ ($r > 0$) region corresponds to the incoming (outgoing) field. From Eq. S7, we have

$$\widetilde{b}_r(t) = \widetilde{b}_{r-vt}(0) - \sqrt{\frac{\kappa_1}{v}}\theta(r)\theta(t - r/v)a(t - r/v), \tag{S8}$$

where $\theta(r)$ is the Heviside step function. We define the input and output operators by

$$\widetilde{b}_{\mathrm{in}}(t) \equiv \widetilde{b}_{-0}(t) = \widetilde{b}_{-vt}(0), \tag{S9}$$

$$\widetilde{b}_{\mathrm{out}}(t) \equiv \widetilde{b}_{+0}(t) = \widetilde{b}_{\mathrm{in}}(t) - \sqrt{\frac{\kappa_1}{v}}a(t). \tag{S10}$$

Using Eqs. S8 and S9, the field operator $\widetilde{b}_r(t)$ at the resonator position ($r = 0$) is given by

$$\widetilde{b}_0(t) = \frac{1}{\sqrt{2\pi}} \int b_k(t)dk = \widetilde{b}_{\text{in}}(t) - \frac{1}{2}\sqrt{\frac{\kappa_1}{v}}a(t). \tag{S11}$$

From the Heisenberg equations of motion for a, we obtain

$$\frac{da}{dt} = -\text{i}[\mathcal{H}_{\text{sys}}(t), a] + \sqrt{v\kappa_1}\widetilde{b}_0 + \sqrt{v\kappa_2}\widetilde{c}_0. \tag{S12}$$

Using Eq. S11 and its counterpart for $\widetilde{c}_0$, Eq. S12 is rewritten as

$$\frac{da}{dt} = -\text{i}[\mathcal{H}_{\text{sys}}(t), a] - \frac{\kappa}{2}a + \sqrt{v\kappa_1}\widetilde{b}_{\text{in}}(t) + \sqrt{v\kappa_2}\widetilde{c}_{\text{in}}(t), \tag{S13}$$

where $\kappa = \kappa_1 + \kappa_2$. Now we switch to a frame rotating at ω_0^{PO} [namely, $a(t)e^{\text{i}\omega_0^{\text{PO}}t} \to a(t)$, $b_{\text{in}}(t)e^{\text{i}\omega_0^{\text{PO}}t} \to b_{\text{in}}(t)$, and $c_{\text{in}}(t)e^{\text{i}\omega_0^{\text{PO}}t} \to c_{\text{in}}(t)$] and drop the rapidly rotating terms in $\mathcal{H}_{\text{sys}}(t)$. Then the static system Hamiltonian is given by

$$\mathcal{H}_{\text{sys}}/\hbar = \frac{\epsilon\omega_0^{\text{PO}}}{2}(a^2 + a^{\dagger 2}) + 6\gamma a^\dagger a^\dagger aa. \tag{S14}$$

Here, we neglected the term $12\gamma a^\dagger a$ which can be regraded as a small renormalization to ω_0^{PO}. From Eqs. S13 and S14, we have

$$\frac{da}{dt} = -\frac{\kappa}{2}a - \text{i}\omega_0^{\text{PO}}\epsilon a^\dagger - 12\text{i}\gamma a^\dagger aa + \sqrt{v\kappa_1}\widetilde{b}_{\text{in}}(t) + \sqrt{v\kappa_2}\widetilde{c}_{\text{in}}(t). \tag{S15}$$

Now we consider the classical amplitude of the resonator field, namely, $\langle a(t)\rangle$. We denote the locking signal applied from the signal port by $E_{\text{s}}(r, t) = E_{\text{s}}^* e^{\text{i}\omega_0^{\text{PO}}(r/v-t)}$. Then, we rigorously have $\langle\widetilde{b}_{\text{in}}(t)\rangle = E_{\text{s}}^*$ and $\langle\widetilde{c}_{\text{in}}(t)\rangle = 0$. Dividing $\langle a(t)\rangle$ into its quadratures as $\langle a(t)\rangle = q_x(t) - \text{i}q_y(t)$, their equations of motion are given by

$$\frac{dq_x}{dt} = -\frac{\kappa}{2}q_x + \omega_0^{\text{PO}}\epsilon q_y - 12\gamma(q_x^2 + q_y^2)q_y + \sqrt{\kappa_1}|E_{\text{s}}|\cos\theta_{\text{s}}, \tag{S16}$$

$$\frac{dq_y}{dt} = -\frac{\kappa}{2}q_y + \omega_0^{\text{PO}}\epsilon q_x + 12\gamma(q_x^2 + q_y^2)q_x + \sqrt{\kappa_1}|E_{\text{s}}|\sin\theta_{\text{s}}, \tag{S17}$$

where $E_{\text{s}} = |E_{\text{s}}|e^{\text{i}\theta_s}$, and we approximated $\langle a^\dagger aa\rangle$ to be $\langle a^\dagger\rangle\langle a\rangle^2$. Equations S16 and S17 can be recast as

$$\frac{dq_x}{dt} = -\frac{\kappa}{2}q_x + \frac{\partial g}{\partial q_y}, \tag{S18}$$

$$\frac{dq_y}{dt} = -\frac{\kappa}{2}q_y - \frac{\partial g}{\partial q_x}, \tag{S19}$$

where

$$g(q_x, q_y) = \frac{\epsilon}{2}\omega_0^{\text{PO}}(q_y^2 - q_x^2) - 3\gamma(q_x^2 + q_y^2)^2 + \sqrt{\kappa_1}|E_{\text{s}}|(q_y\cos\theta_{\text{s}} - q_x\sin\theta_{\text{s}}). \tag{S20}$$

Considering that $P_{\text{p}}/P_{\text{p0}} = (\epsilon/\epsilon_0)^2$, where $\epsilon_0 = \kappa/(2\omega_0^{\text{PO}})$ is the threshold for ϵ, these are Eqs. 2 to 4 in the main article.

B. Master equation

We denote the resonator transition operator by $s_{mn} = |m\rangle\langle n|$, where $|m\rangle$ and $|n\rangle$ are the Fock states. Its Heisenberg equation is given, in the rotating frame [$s_{mn}(t)e^{\text{i}\omega_0^{\text{PO}}(n-m)t} \to s_{mn}(t)$], by

$$\begin{aligned}
\frac{d}{dt}s_{mn} &= \frac{\text{i}}{\hbar}[\mathcal{H}_{\text{sys}}, s_{mn}] + \frac{\kappa}{2}(2a^\dagger s_{mn}a - s_{mn}a^\dagger a - a^\dagger as_{mn}) \\
&\quad + \sqrt{v\kappa_1}[s_{mn}, a^\dagger]\widetilde{b}_{\text{in}}(t) - \sqrt{v\kappa_1}\widetilde{b}_{\text{in}}^\dagger(t)[s_{mn}, a] \\
&\quad + \sqrt{v\kappa_2}[s_{mn}, a^\dagger]\widetilde{c}_{\text{in}}(t) - \sqrt{v\kappa_2}\widetilde{c}_{\text{in}}^\dagger(t)[s_{mn}, a].
\end{aligned} \tag{S21}$$

where the static system Hamiltonian $\mathcal{H}_{\text{sys}}$ is given by Eq. S14. Using again that $\langle \widetilde{b}_{\text{in}}(t) \rangle = E_{\text{s}}^*$ and $\langle \widetilde{c}_{\text{in}}(t) \rangle = 0$, $\langle s_{mn} \rangle$ evolves as

$$
\begin{aligned}
\frac{d}{dt}\langle s_{mn} \rangle \;=\; & \frac{\mathrm{i}\omega_0^{\text{PO}}\epsilon}{2}\Big(\sqrt{m(m-1)}\langle s_{m-2,n}\rangle + \sqrt{(m+1)(m+2)}\langle s_{m+2,n}\rangle \\
& -\sqrt{n(n-1)}\langle s_{m,n-2}\rangle - \sqrt{(n+1)(n+2)}\langle s_{m,n+2}\rangle \Big) \\
& +6\mathrm{i}\gamma[m(m-1)-n(n-1)]\langle s_{mn}\rangle + \frac{\kappa}{2}\Big[2\sqrt{(m+1)(n+1)}\langle s_{m+1,n+1}\rangle - (m+n)\langle s_{mn}\rangle \Big] \\
& +\sqrt{\kappa_1}E_{\text{s}}\Big(\sqrt{n}\langle s_{m,n-1}\rangle - \sqrt{m+1}\langle s_{m+1,n}\rangle \Big) \\
& -\sqrt{\kappa_1}E_{\text{s}}^*\Big(\sqrt{n+1}\langle s_{m,n+1}\rangle - \sqrt{m}\langle s_{m-1,n}\rangle \Big),
\end{aligned}
\tag{S22}
$$

where we have used $a^\dagger s_{mn} a = \sqrt{(m+1)(n+1)}\,s_{m+1,n+1}$ and similar equalities.

Since $\langle s_{mn}\rangle = \text{Tr}[\rho s_{mn}] = \rho_{nm}$, Eq. S22 is equivalent to the following master equation,

$$
\frac{d\rho}{dt} = -\frac{\mathrm{i}}{\hbar}[\mathcal{H}_{\text{int}}, \rho] + \frac{\kappa}{2}(2a\rho a^\dagger - a^\dagger a \rho - \rho a^\dagger a),
\tag{S23}
$$

where

$$
\mathcal{H}_{\text{int}}/\hbar = \frac{\epsilon\omega_0^{\text{PO}}}{2}(a^2 + a^{\dagger 2}) + 6\gamma a^\dagger a^\dagger a a + \mathrm{i}\sqrt{\kappa_1}|E_{\text{s}}|(e^{\mathrm{i}\theta_s}a^\dagger - e^{-\mathrm{i}\theta_s}a).
\tag{S24}
$$

By introducing dimensionless time $\tau = t\kappa/2$, Eq. S23 becomes

$$
\frac{d\rho}{d\tau} = -\mathrm{i}[\mathcal{H}'_{\text{int}}, \rho] + (2a\rho a^\dagger - a^\dagger a \rho - \rho a^\dagger a).
\tag{S25}
$$

Here the dimensionless Hamiltonian $\mathcal{H}'_{\text{int}}$ is given by

$$
\mathcal{H}'_{\text{int}} = \mathcal{H}_{\text{int}}/(\hbar\kappa/2) = \gamma' a^\dagger a^\dagger a a + \frac{1}{2}\sqrt{\frac{P_{\text{p}}}{P_{\text{p0}}}}(a^2 + a^{\dagger 2}) + \mathrm{i}\sqrt{N^{\text{PO}}}(e^{\mathrm{i}\theta_s}a^\dagger - e^{-\mathrm{i}\theta_s}a),
\tag{S26}
$$

where $\gamma' = 12\gamma/\kappa$, $\sqrt{N^{\text{PO}}} = \sqrt{\kappa_1}|E_{\text{s}}|/(\kappa/2)$.

We numerically solve Eq. S25 by expanding ρ in the number state basis [3], namely $\rho = \sum_{m,n=0}^{N}\rho_{mn}|m\rangle\langle n|$, and calculate the Q function $Q(z) = \langle z|\rho|z\rangle/\pi$, where z is a coherent state [2].

C. Experimental parameters

To simulate the experiments, we need to determine the parameters such as N^{PO}, P_{p0}, and γ. N^{PO} is determined from the above definition and $|E_{\text{s}}| = \sqrt{P_{\text{s}}^{\text{PO}}/\hbar\omega_0^{\text{PO}}}$. Since we do not precisely know the mutual inductance between the pump line and the SQUID loop in the PPLO, we can only roughly determine P_{p0}, the threshold for the pump power, from the measurement shown in Fig. 2a in the main article, and leave it as a semi-adjustable parameter. γ is calculated based on the theory in Ref. 4. It is related with the wavenumber k of the first mode of the CPW resonator terminated by a SQUID,

$$
\gamma = -\Big(\frac{2\pi}{\Phi_0}\Big)^2 \frac{\hbar B_k}{8C_k},
\tag{S27}
$$

where

$$
B_k = \frac{(1/4)\cos^2(kd)}{1 + 2kd/\sin(2kd)},
\tag{S28}
$$

$$
C_k = \frac{C_{\text{cav}}}{2}\Big[1 + \frac{\sin(2kd)}{2kd}\Big] + C_{\text{J}}\cos^2(kd).
\tag{S29}
$$

Here, d and C_{cav} are the length and the total capacitance of the CPW resonator, respectively, and C_{J} is the total junction capacitance of the SQUID. The flux dependent resonant frequency is given by

$$
\omega_0^{\text{PO}}(\Phi_{\text{sq}}) = \frac{1}{\sqrt{L_k(C_k + C_{\text{in}}^{\text{PO}})}},
\tag{S30}
$$

where

$$1/L_k = \frac{(kd)^2}{2L_{\mathrm{cav}}}\left[1 + \frac{\sin(2kd)}{2kd} + \frac{2C_{\mathrm{J}}}{C_{\mathrm{cav}}}\cos^2(kd)\right].\tag{S31}$$

Here, L_{cav} is the total inductance of the CPW resonator, and kd is determined by the equation [4],

$$kd\tan(kd) = \left(\frac{2\pi}{\Phi_0}\right)L_{\mathrm{cav}}2I_0\left|\cos\left(\pi\frac{\Phi_{\mathrm{sq}}}{\Phi_0}\right)\right| - \frac{C_{\mathrm{J}}}{C_{\mathrm{cav}}}(kd)^2,\tag{S32}$$

where I_0 represents the critical current of each of the SQUID JJ.

We fit the data shown in Fig. S6 by Eq. S30 with fitting parameters of I_{c} and C_{cav}, which are determined to be 3.1 μA and 410 fF, respectively. Using Eqs. S27 to S29, and S32, we calculate γ to be -2.3×10^5 Hz at $\omega_0^{\mathrm{PO}}/2\pi = 10.51$ GHz.

D. Simulation of non-locking error

Figure S7a shows an example of the calculated Q function. The parameters used in the calculation are $P_{\mathrm{p}}/P_{\mathrm{p0}} = 1.660$ (2.2 dB), $N^{\mathrm{PO}} = 0.09$, $\theta_{\mathrm{s}} = \pi/2$. The density matrix is truncated at $N = 80$, which we confirmed large enough for these parameters. Also, the calculation is stopped at $\tau = 20$, which we confirmed long enough for the system to become stationary. We clearly observe two distribution peaks, which correspond to 0π and 1π states of PPLO. Based on this result, we get the probability of 0π state by integrating Q for $q_x > 0$. Figure S7b shows the probability of 0π state as a function of the LS phase for different N^{PO}'s. N^{PO}'s are chosen from those in Fig. 2d in the main article. The agreement is fairly good.

[1] Lin, Z. R. *et al.* Single-shot readout of a superconducting flux qubit with a flux-driven Josephson parametric amplifier. *Appl. Phys. Lett.* **103**, 132602 (2013).

[2] Walls, D. F. & Milburn, G. J. *Quantum optics* (Springer-Verlag, Berlin, Tokyo, 1994).

[3] Johansson, J., Nation, P. & Nori, F. Qutip 2: A Python framework for the dynamics of open quantum systems. *Computer Physics Communications* **184**, 1234 – 1240 (2013).

[4] Wallquist, M., Shumeiko, V. S. & Wendin, G. Selective coupling of superconducting charge qubits mediated by a tunable stripline cavity. *Phys. Rev. B* **74**, 224506 (2006).
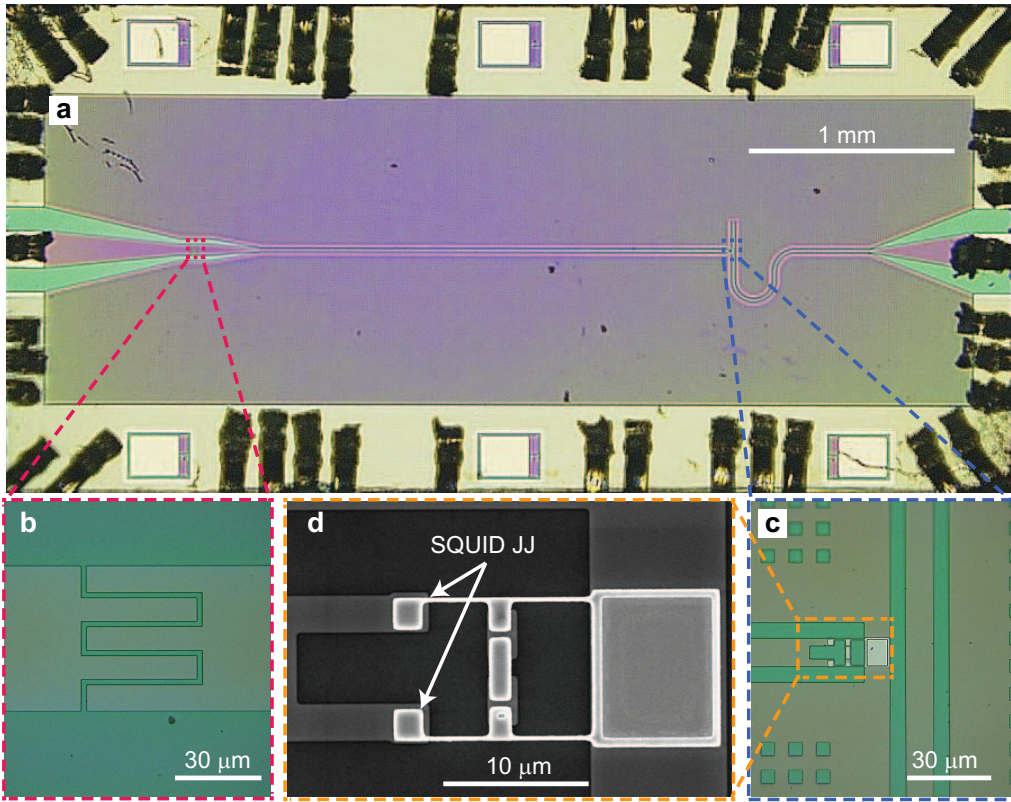
FIG. S1: Images of the parametric phase-locked oscillator. **a,** Optical image of the device. The $\lambda/4$-type CPW resonator is made of 150-nm-thick niobium film deposited on an oxidized silicon substrate. **b,** Magnified image of the coupling capacitance. **c,** Magnified optical image of the dc-SQUID part and **d,** its scanning electron micrograph. The SQUID loop contains a three-Josephson-junction flux qubit, which is not used in this work.
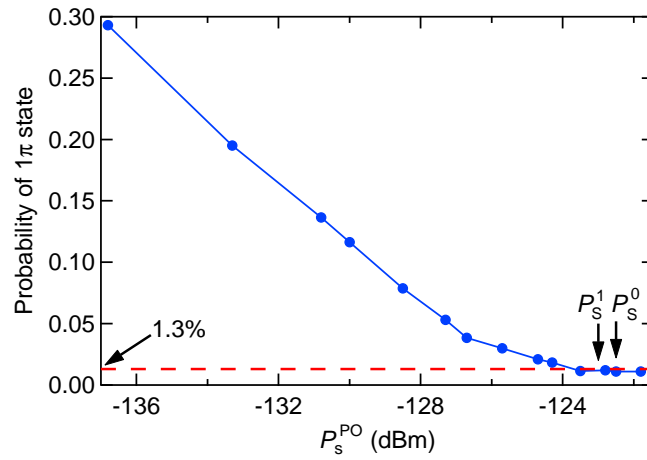

FIG. S2: Minimum probability of 1π state as a function of the locking-signal power. The non-zero minimum probability indicated by the horizontal dashed line is due to the initialization error of the qubit. P_s^0 and P_s^1 represent the microwave powers injected into the PPLO when the qubit is in $|0\rangle$ state and in $|1\rangle$ state, respectively.
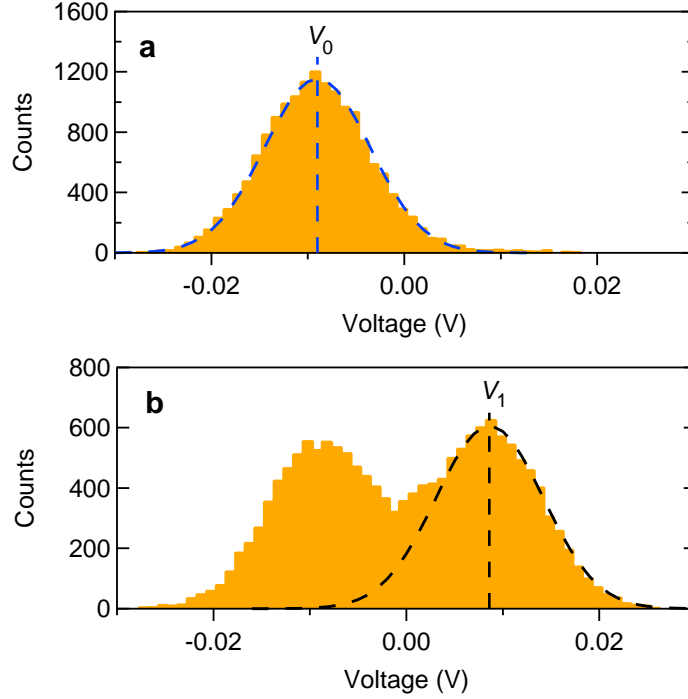
FIG. S3: Histograms of the voltage of the reflected readout pulse **a**, with qubit-control π pulse off and **b**, on. The input power to the JPA is -122.5 dBm, which is the same as in the Rabi-oscillation measurement in the main article. The JPA is operated at a gain of 13 dB and a bandwidth of 21 MHz with 1-dB-compression point of -123 dBm. The dashed lines represent the Gaussian fits to the distribution peaks to extract the mean values of $V_0 = -0.090$ V and $V_1 = 0.086$ V. Only right-hand side of the peak is fitted for **b**.
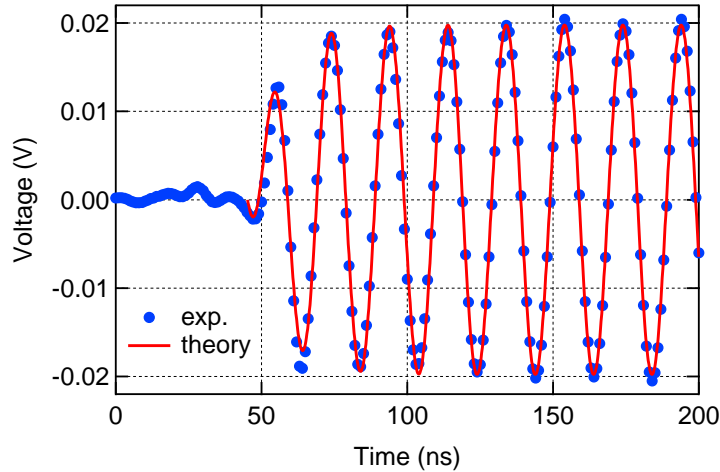

FIG. S4: Time trace of the PPLO output signal. $\omega_{\mathrm{p}}/2\pi = 2 \times 10.193$ GHz, $t_{\mathrm{p}} = 30$ ns, $t_{\mathrm{r}} = 50$ ns, and $N^{\mathrm{r}} = 5.5$ (See main article for definitions). The output signal at $\omega_{\mathrm{p}}/2$ is down-converted to $\omega_{\mathrm{IF}} = 2\pi \times 50$ MHz, and digitized at 1 GS/s. Qubit-control π pulse is turned on ($t_{\mathrm{c}} = 10$ ns). We selected 9250 traces which are in 1π-phase state and averaged them (blue circles). Solid curve represents a fit to the data for $t > t_0 = 45$ ns. We assumed a function $V(t) = A(1 - e^{-(t-t_0)/\tau}) \cos(\omega_{\mathrm{IF}} t + \phi_0)$, and obtained the time constant τ of 9.4 ns.
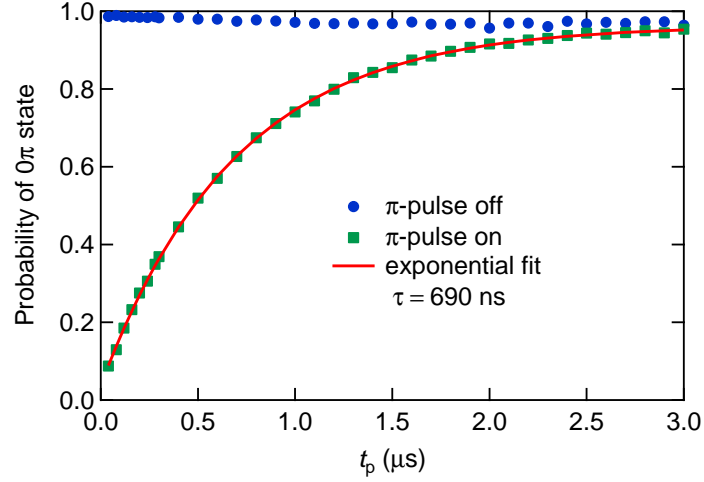
FIG. S5: Probability of 0π-state as a function of the delay time $t_{\rm p}$ between the readout and pump pulses with qubit-control π-pulse on (green square) and off (blue circle). The pulse sequence is shown in Fig. 4a in the main article. Here, $t_{\rm c} = 10$ ns, $t_{\rm r} = 50$ ns, and $t_{\rm d} = 300$ ns. The solid curve is an exponential fit with a time constant of 690 ns.
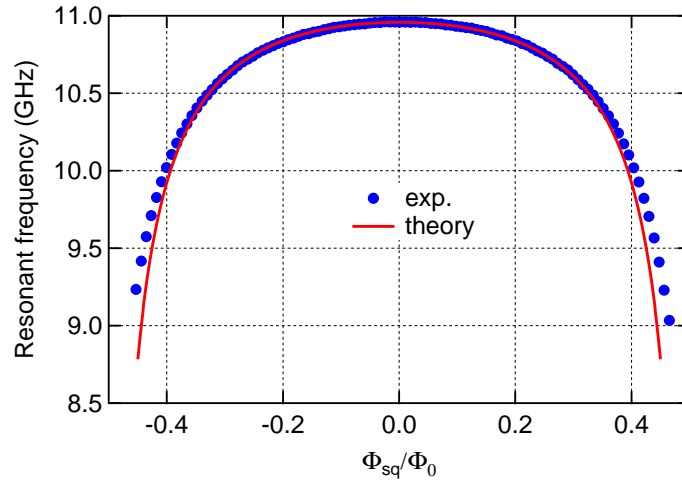

FIG. S6: Resonant frequency $\omega_0^{\rm PO}$ as a function of the flux bias $\Phi_{\rm sq}$. Solid circles represent the experimental data, and the solid curve is a theoretical fit (Eq. S30) to the data for $|\Phi_{\rm sq}/\Phi_0| \leq 0.32$. In the fitting, we assumed $L_{\rm cav}$ of 1.08 nH, $C_{\rm in}^{\rm PO}$ of 15 fF, and $C_{\rm J}$ of 50 fF, which are designed values. The deviation of the fitting outside the above range could be due to the loop inductance of the SQUID, which is neglected in the theory and estimated to be ~ 40 pH by the simulation.
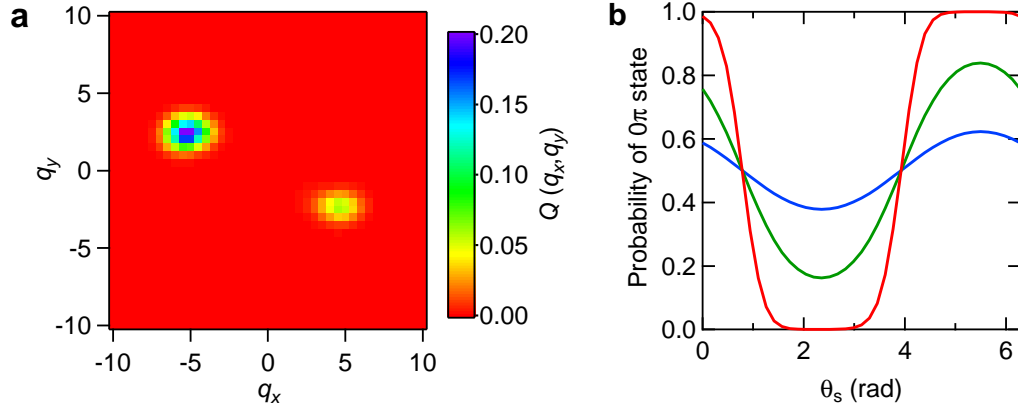
FIG. S7: Results of the numerical calculation. **a,** Example of the calculated Q function. The parameters used in the calculation are $P_\mathrm{p}/P_\mathrm{p0} = 1.660$ (2.2 dB), $N^\mathrm{PO} = 0.09$, $\theta_\mathrm{s} = \pi/2$. The density matrix is truncated at $N = 80$, and the calculation is stopped at $\tau = 20$. **b,** Probability of 0π state as a function of the locking signal phase θ_s for $N^\mathrm{PO} = 0.009$ (blue), $N^\mathrm{PO} = 0.09$ (green), and $N^\mathrm{PO} = 0.9$ (red). Other parameters used in the calculation are the same as in **a**.